



HAL
open science

Large-scale network dynamics underlying the first few hundred milliseconds after stimulus presentation: An investigation of visual recognition memory using iEEG

Jakub Kopal, Jaroslav Hlinka, Elodie Despouy, Luc Valton, Marie Denuelle, Jean-christophe Sol, Jonathan Curot, Emmanuel J Barbeau

► To cite this version:

Jakub Kopal, Jaroslav Hlinka, Elodie Despouy, Luc Valton, Marie Denuelle, et al.. Large-scale network dynamics underlying the first few hundred milliseconds after stimulus presentation: An investigation of visual recognition memory using iEEG. *Human Brain Mapping*, 2023, 44 (17), pp.5795-5809. 10.1002/hbm.26477 . hal-04699038

HAL Id: hal-04699038

<https://ut3-toulouseinp.hal.science/hal-04699038v1>

Submitted on 16 Sep 2024

HAL is a multi-disciplinary open access archive for the deposit and dissemination of scientific research documents, whether they are published or not. The documents may come from teaching and research institutions in France or abroad, or from public or private research centers.


L'archive ouverte pluridisciplinaire **HAL**, est destinée au dépôt et à la diffusion de documents scientifiques de niveau recherche, publiés ou non, émanant des établissements d'enseignement et de recherche français ou étrangers, des laboratoires publics ou privés.



Distributed under a Creative Commons Attribution - NonCommercial - NoDerivatives 4.0 International License

RESEARCH ARTICLE

Large-scale network dynamics underlying the first few hundred milliseconds after stimulus presentation: An investigation of visual recognition memory using iEEG

Jakub Kopal^{1,2,3} | Jaroslav Hlinka^{1,4}  | Elodie Despouy³ | Luc Valton^{3,5} | Marie Denuelle^{3,5} | Jean-Christophe Sol^{5,6} | Jonathan Curot^{3,5} | Emmanuel J. Barbeau³

¹Institute of Computer Science of the Czech Academy of Sciences, Prague, Czech Republic

²Department of Computing and Control Engineering, University of Chemistry and Technology, Prague, Czech Republic

³Centre de Recherche Cerveau et Cognition, Toulouse III University – CNRS UMR 5549, Toulouse, France

⁴National Institute of Mental Health, Klecany, Czech Republic

⁵University Hospital Purpan, Toulouse, France

⁶Toulouse NeuroImaging Center, Toulouse, France

Correspondence

Emmanuel J. Barbeau, Centre de Recherche Cerveau & Cognition (CerCo – UMR5549), CNRS, Université de Toulouse, CHU Purpan, Pavillon Baudot, 31059 Toulouse cedex 9, France.

Email: emmanuel.barbeau@cnrs.fr

Funding information

Campus France, Grant/Award Number: 44815QG; Grantová Agentura České Republiky, Grant/Award Number: 19-11753S; Ministerstvo Zdravotnictví České Republiky, Grant/Award Number: 00023752; Vysoká Škola Chemicko-technologická v Praze, Grant/Award Number: A2 FCHI 2018 012

Abstract

Recognition memory is the ability to recognize previously encountered objects. Even this relatively simple, yet extremely fast, ability requires the coordinated activity of large-scale brain networks. However, little is known about the sub-second dynamics of these networks. The majority of current studies into large-scale network dynamics is primarily based on imaging techniques suffering from either poor temporal or spatial resolution. We investigated the dynamics of large-scale functional brain networks underlying recognition memory at the millisecond scale. Specifically, we analyzed dynamic effective connectivity from intracranial electroencephalography while epileptic subjects ($n = 18$) performed a fast visual recognition memory task. Our data-driven investigation using Granger causality and the analysis of communities with the Louvain algorithm spotlighted a dynamic interplay of two large-scale networks associated with successful recognition. The first network involved the right visual ventral stream and bilateral frontal regions. It was characterized by early, predominantly bottom-up information flow peaking at 115 ms. It was followed by the involvement of another network with predominantly top-down connectivity peaking at 220 ms, mainly in the left anterior hemisphere. The transition between these two networks was associated with changes in network topology, evolving from a more segregated to a more integrated state. These results highlight that distinct large-scale brain networks involved in visual recognition memory unfold early and quickly, within the first 300 ms after stimulus onset. Our study extends the current understanding of the rapid network changes during rapid cognitive processes.

KEYWORDS

connectivity, dynamics, intracranial EEG, network, recognition memory

This is an open access article under the terms of the [Creative Commons Attribution-NonCommercial-NoDerivs](https://creativecommons.org/licenses/by-nc-nd/4.0/) License, which permits use and distribution in any medium, provided the original work is properly cited, the use is non-commercial and no modifications or adaptations are made.

© 2023 The Authors. *Human Brain Mapping* published by Wiley Periodicals LLC.

1 | INTRODUCTION

Visual recognition memory is the ability to recognize previously encountered objects. This type of declarative memory has been studied since the 1960s (Milner, 1972), with numerous findings revealing how accurate (Brady et al., 2008), fast (Besson et al., 2012), and long-lasting (Larzabal et al., 2018) it can be. These studies have also pinpointed the medial temporal lobes (MTL), specifically the perirhinal cortex and the hippocampus, as critical for successful recognition memory (Brown & Aggleton, 2001; Eichenbaum et al., 2007; Staresina et al., 2012). Alongside the MTL, visual recognition memory also depends on the “what” system: the visual ventral stream involving temporo-basal brain regions such as the lingual, fusiform, and parahippocampal gyri (DiCarlo et al., 2012). The participation of the ventral stream is asymmetric, as visual recognition memory relies more on the ventral stream in the right hemisphere than in the left hemisphere (Barbeau et al., 2008; Elger et al., 1997; Guerin & Miller, 2009; Patterson & Bradshaw, 1975; Petrovska et al., 2021). In addition, visual recognition memory also involves parietal and frontal lobe regions in both hemispheres for a host of processes related to confidence, decision-making, attention to memory, meta-memory, and behavioral response (Bastin et al., 2019 for a review; Gonzalez et al., 2015; Hoppstädter et al., 2015; Petrovska et al., 2021). Therefore, even a simple task, such as deciding whether an object has already been seen, involves a large number of brain regions throughout the entire brain.

The activity of individual brain regions underlying recognition memory has been extensively described in prior literature (Despouy et al., 2020). Although the first behavioral responses occur around 360 ms (Besson et al., 2012), the first neural differences between targets and distractors are already identified around 200 ms (Barbeau et al., 2008; Barragan-Jason et al., 2015). Yet, many different brain regions are involved for up to 600 ms or more. Visual recognition memory thus recruits many regions across the brain within a fraction of a second.

However, brain regions do not operate in isolation but are interconnected in large-scale networks (Varela et al., 2001). The basis of every network is connectivity, defined as either anatomical links (structural connectivity), statistical dependencies (functional connectivity), or causal interactions (effective connectivity) (Sporns, 2007). Substantial evidence supports the hypothesis that brain network architecture is non-random and optimized to support cognitive abilities (Sporns, 2011). Brain networks are designed for effective information processing and synthesis by balancing local segregation of function and global integration of information. Given the continually evolving environment and depending on the system's demands, there are continuously changing interaction patterns between brain regions (Bassett et al., 2011). Therefore, both the topology of the networks and their interactions are highly dynamic (Hutchison et al., 2013; Shine et al., 2016). It is generally assumed that their reconfigurations are driven by higher-order cognitive control systems involving the frontal lobes (Braun et al., 2015). Moreover, dynamic reconfiguration is directly linked to cognitive performance during memory (Cohen & D'Esposito, 2016; Meunier et al., 2014). Consequently, the field has

evolved toward a strong interest in the dynamic reorganization of brain networks (Preti et al., 2017), sometimes called functional chronotomics (Calhoun et al., 2014). However, current studies of large-scale network dynamics are primarily based either on fMRI or scalp electroencephalography (EEG) and thus suffer from limited ability to precisely identify the timing and dynamics of brain activity (temporal resolution) or the location of brain activity (spatial resolution).

One puzzling question in this context is what are the sub-second brain network dynamics supporting cognitive abilities that unfold as quickly as recognition memory? Despite how critical they are, little is known about network organization and topology underlying these first few hundred milliseconds of cognitive processes.

To achieve the spatial and temporal resolution needed for such a study, we analyzed intracranial EEG (iEEG) recorded while epileptic patients underwent a visual recognition memory task. To assess brain network dynamics, we computed effective connectivity using multivariate Granger causality for all pairs of iEEG channels. We then examined the temporal evolution of whole-brain network topology. Specifically, network topology was characterized by measures of dynamic network integration and segregation. Furthermore, we studied the connectivity dynamics of brain networks identified using data-driven techniques. In addition, we tested whether the networks were driven by bottom-up processes, as is classically known about rapid visual processing (DiCarlo et al., 2012 for a review; Rousselet et al., 2004; VanRullen & Thorpe, 2001). Finally, we probed how the observed dynamics were associated with performance during the visual recognition memory task and with successful memory recognition.

2 | MATERIALS AND METHODS

2.1 | Experimental design

This study was approved by the Toulouse University Hospital Ethics Committee (CER No. 47-0913). All patients signed informed consent for the study.

2.2 | Participants

iEEG was recorded for 18 subjects with drug-refractory epilepsy (8 women, age: 37.61 ± 11.37 years old; Table 1). The subjects were admitted to the Epilepsy Monitoring Unit at Toulouse University Hospital for the identification and possible subsequent resection of the epileptogenic zone. In each subject, 8–13 depth electrodes were stereotactically implanted. The depth electrodes were 0.8 mm in diameter and contained 8–18 platinum/iridium contacts, each 2 mm long (Microdeep depth electrode, DIXI Medical, France). Each implantation was individually tailored to the seizure onset zone, and the placement of each depth electrode was based exclusively on clinical criteria, independently of this study. Patients remain hospitalized for 1–2 weeks until they have had one or more spontaneous seizures. The visual recognition memory task was proposed to them generally 2–

TABLE 1 Participants' information and performance.

Sex	Age	Dominant hand	Language laterality	% contacts in L hemisphere	Successful trials	d-prime	minRT
F	42	R	L	47	166	0.92	480
M	59	R	x	60	152	1.70	420
M	35	R	L	40	150	1.57	450
M	21	R	L	17	198	2.54	390
M	24	L	L	63	171	1.43	480
M	34	L	L	0	198	1.39	420
F	63	L	R	20	176	1.50	510
F	32	R	L	63	104	1.21	480
F	31	A	L	77	163	1.70	450
F	33	L	R	63	208	2.03	420
M	47	A	L	87	195	1.22	420
M	41	R	L	73	100	2.47	510
M	21	L	L	100	84	1.21	420
M	40	R	L	67	131	1.22	420
F	37	R	L	53	164	1.74	450
F	50	x	x	27	194	1.92	420
M	39	x	x	73	64	1.45	420
F	28	x	x	97	214	2.00	390

Note: Table summarizing available information about the subjects who participated in this study, including biological sex, age, dominant hand, language laterality, and the number of successful trials recorded. Since the electrode implantation varied significantly across subjects, we report the percentage of contacts in the left hemisphere. Finally, we include two measures of test performance: minimal reaction time: the moment when the number of hits is significantly higher than the number of false alarms (minRT) and d-prime.

3 days after the implantation, allowing ample time to recover from the effect of anesthesia.

Intracranial EEG activity was recorded using two synchronized 64-channel acquisition systems (SystemPlus Evolution, SD LTM 64 EXPRESS, Micromed, France) with a sampling frequency of 256 Hz for two patients and either 1024 or 2048 Hz for the others (high pass-filter: 0.15 Hz). None of the patients had a seizure within 6 h before the recordings. The preoperative MRI and postoperative CT images were fused and normalized to the Montreal Neurological Institute (MNI) brain atlas for precise contact localization.

To ensure an equal number of channels for each patient, we manually selected channels localized in the grey matter (based on MRI images) and on which we could visually recognize event-related potentials induced by stimuli presentation. Furthermore, we only included bipolar channels that did not share a common contact to avoid spuriously high connectivity. Therefore, using this a priori selection, we analyzed 18 subjects with 30 channels per subject. The summary of data quality for the selected and excluded channels is available in Figure S1.

2.3 | Visual recognition memory test

Each subject performed a speeded visual recognition memory task, namely the speed and accuracy boosting procedure (SAB; Besson

et al., 2012), while their iEEG was being recorded (Figure 1). The SAB test is demanding and requires one or two training sessions, which were not included in subsequent analyses. Patients participated in 7–10 blocks depending on their willingness and availability. Each block began with an encoding phase, during which 30 trial-specific stimuli (targets) were presented individually for at least 3 s (self-paced) in the center of a gray screen. The stimuli were taken from an extensive database of high-quality cropped photos of everyday objects. Participants were explicitly instructed to remember all stimuli. A distracting phase followed, during which subjects watched a colored cartoon video with sound on for 3 min. Finally, the recognition memory phase consisted of presenting the 30 targets and 30 distractors. Subjects were required to respond to the targets by raising their finger from an infrared pad. A response deadline between 500 and 800 ms, depending on the patient's cognitive ability, was set, while audio feedback motivated subjects to answer as quickly and accurately as possible. Responses were based on a go/no-go design. If a go response was given before the response time limit, positive audio feedback was played if the stimulus was a target (Hit), or negative feedback was provided if it was a distractor (False alarm). If a no-go response was given, positive audio feedback was played if the stimulus was a distractor (Correct rejection), or negative feedback was provided if the stimulus was a target (Miss). The intertrial-fixation period was 800–1100 ms. We analyzed only the first 64 Hits and Correct rejections trials in this study (maximum number of successful trials available for

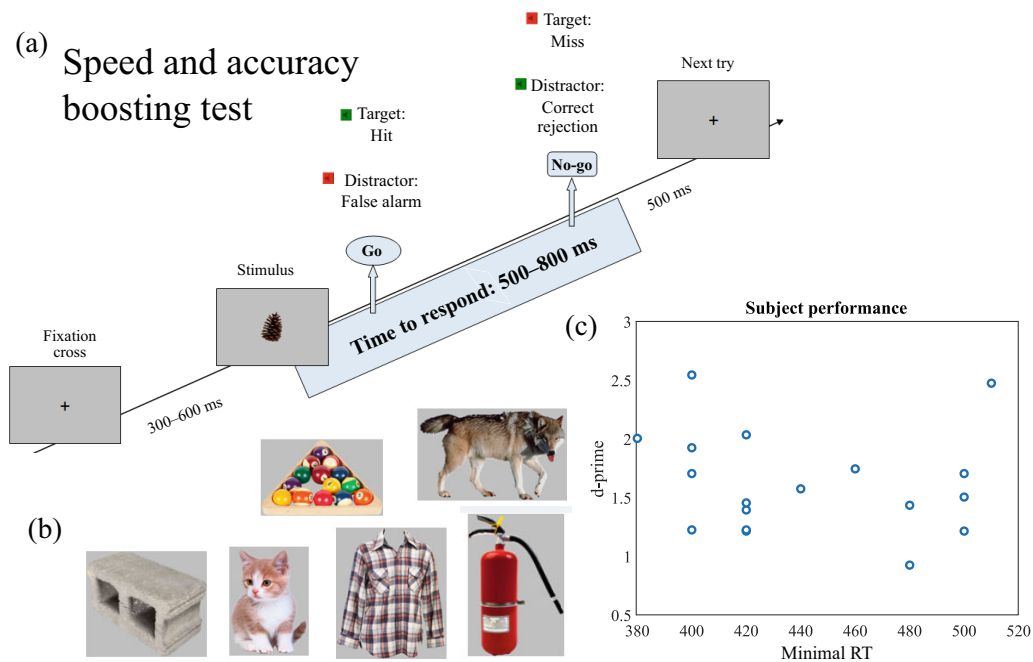


FIGURE 1 SAB test illustration and participant's performances. Eighteen subjects underwent the speed and accuracy boosting procedure (SAB), a speeded visual recognition memory task, while iEEG was recorded. (a) SAB test procedure. Illustration of the SAB go/no-go testing design with a response deadline of between 500 and 800 ms. We analyzed only Hits and Correct rejections in this analysis. (b) SAB test stimuli. The stimuli used in the encoding phase were high-quality cropped photos of everyday objects. (c) SAB test performance. Each participant's performance is characterized by a time of reaction and test performance, namely by minimal reaction time and d-prime.

all subjects). The varying response time, aiming at facilitating the task for the patients, did not change the minimal reaction time compared with a group of healthy subjects as analyzed in a previous study (Data S1, Despouy et al., 2020).

We evaluated each subject's performance using two discrimination indices. First, the subject's performance was characterized using d-prime (difference in z-transforms of Hit rate and False alarm rate) (Rousselet et al., 2004). Second, the minimal reaction time (minRT), summarizing the speed of response, was defined as the minimal processing time required to recognize targets. minRT was computed by determining the latency at which correct go responses (Hits) started to significantly outnumber incorrect go responses (false alarms) (Besson et al., 2012). As in other studies, we used 20 ms time bins and a Fisher's exact test ($p < .05$), followed by at least two significant consecutive bins to compute the minRT (Despouy et al., 2020).

2.4 | Connectivity analyses

2.4.1 | iEEG preprocessing

We used a bipolar montage between adjacent contacts to remove artifact contaminations, identify local activations, and provide a reference-free representation of the phenomena under observation (Lachaux et al., 2003). Visual inspection of the EEG of all trials, as well

as manual artifact rejection procedures, were used to reject interictal activities period. The inspection was performed by ED, a trained PhD student, supervised by JC, an epileptologist from the Toulouse University Hospital. This standard procedure led to exclusion of 14% of all trials on average across participants (range: 8%–22%) with interictal epileptiform activity, a percentage similar to previous studies. This procedure decreased the risk of including trials modified by epileptic activity. Finally, we downsampled each channel to 256 Hz (original sampling frequency for two subjects).

Across all subjects, we analyzed 540 channels (Figure 2a), 308 of which were in the left and 232 in the right hemispheres. Each recording channel was assigned to one of 90 regions of the AAL atlas (Tzourio-Mazoyer et al., 2002) based on its MNI coordinates using the SPM12 software package (Wellcome Department of Cognitive Neurology, London, UK) and the Anatomy toolbox (Eickhoff et al., 2005; Figure 2b). All data were processed with MATLAB (Version 9.1.0, The MathWorks Inc, Natick, MA).

2.4.2 | Connectivity estimation

We investigated dynamic effective connectivity covering the temporal segment from 200 ms pre-stimulus baseline to 800 ms after stimulus onset. We performed sliding-window connectivity analyses using windows with a length of 64 samples (250 ms) and a shift of 4 samples (similar results were obtained with a window of 16 samples). Each

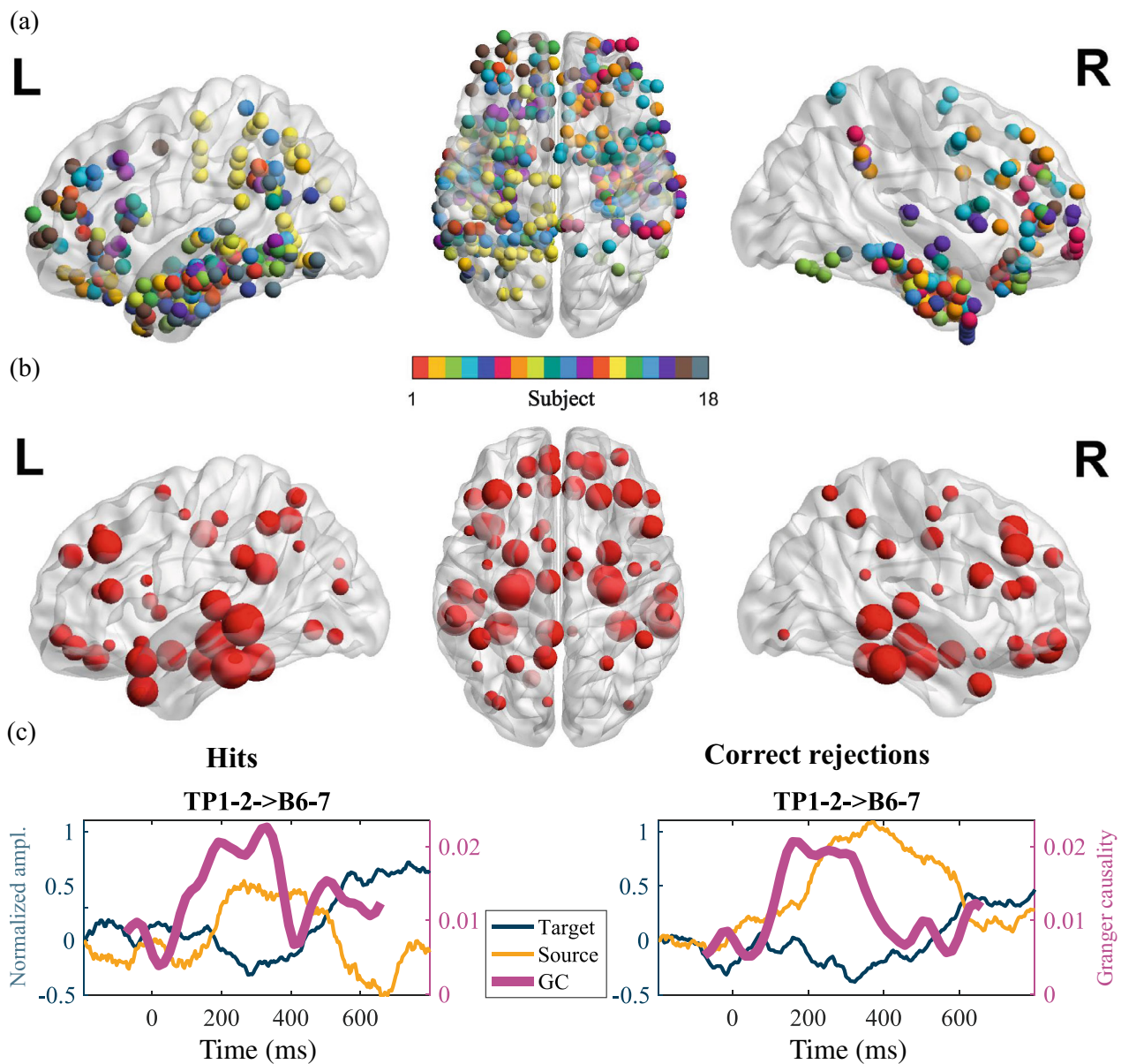


FIGURE 2 iEEG recordings and effective connectivity. We calculate effective connectivity between each pair of 30 channels separately for each of the 18 subjects totaling 15,600 unique electrode pairs. (a) Overview of all recording locations across subjects. Each subject's brain activity was monitored using multiple intracranial depth electrodes that targeted different brain regions. The different colors correspond to different subjects. (b) Mapping channels to AAL atlas. In order to generalize across subjects, we mapped each recording channel to the AAL atlas region based on its MNI coordinates. In total, the channels covered 68 out of 90 possible regions, with a different number of channels sampled from each region. The size of each sphere corresponds to the sampling density of the region. (c) Dynamic effective connectivity example. Using sliding windows, we calculated dynamic Granger causality (i.e., effective connectivity) for all channel pairs (e.g., TP1-2 and B6-7) separately for the Hits and Correct rejection trials. According to the definition of Granger causality, the source influences the target.

sliding window was multiplied by a Hanning window to suppress spurious connectivity and reduce sensitivity to outliers (Preti et al., 2017).

Effective connectivity

We used dynamic multivariate Granger causality (MVGC) to estimate the EC between channels. It implements a statistical, predictive notion of causality, whereby causes precede and help to predict their effects.

Classical Granger causality from Y to X can be formally written as the log-likelihood ratio:

$$F_{Y \rightarrow X} = \ln \frac{\Sigma_1}{\Sigma_2}$$

$$\Sigma_1 = \text{var}(\epsilon_{1t}), \Sigma_2 = \text{var}(\epsilon_{2t})$$

$$X_t = \sum_{j=1}^M a_j X_{t-j} + \varepsilon_{1t}$$

$$X_t = \sum_{j=1}^M a_j X_{t-j} + \sum_{j=1}^M b_j Y_{t-j} + \varepsilon_{2t}$$

where X and Y represent recorded time series, a_j and b_j are parameters of the autoregressive process corresponding to time lag j , ε_1 and ε_2 represent residuals of the autonomous and coupled system, respectively, and M is the model order (we used a constant order of 10, but similar results were observed using orders of 5 or 15).

In this manuscript, the F-statistic represented the magnitude of Granger causality. The F statistic is computed as the ratio of the mean square of residuals from the restricted model to the mean square of residuals from the unrestricted model. Therefore, the F-statistic was strictly positive. In addition, the use of a multivariate extension of Granger causality ensured the control for common causal influences (Seth et al., 2015).

Since our testing paradigm was time-constrained, we used relatively short time windows for the dynamic connectivity analysis. Therefore, estimating the multivariate autoregressive model parameters is potentially challenging due to the use of short time series. Nevertheless, we overcame this difficulty through the “vertical regression” implemented in the freely available toolbox from Barnett and Seth (2014) that addresses short time windows when multiple trials are available. In particular, this method assumes that each trial is an independent realization of the same underlying stochastic generative process. Therefore, we ended up with only one MVGC model across all trials for each subject (Figure 2c).

2.5 | Bottom-up and top-down directions

Granger causality is a directed measure that allows for assessing the direction of interactions. The key neurocognitive question is the role of top-down and bottom-up information flow in neural networks. Based on the definition given by Gaillard et al. (2009), the bottom-up (feedforward) direction is the causal influence of posterior channels onto the more anterior channel and vice versa for the top-down (feedback) direction. If their y coordinates were identical, bottom-up was defined as the causal influence of the lower onto the higher channel based on the z coordinates (this occurred in 3% of the cases).

2.5.1 | Statistical analyses

It is important to stress that studies using iEEG face several challenges, such as the relatively low number of subjects, short time windows, and tailored implantations that offer only a limited sampling of brain areas (see Pidnebesna et al., 2022 for more details concerning the challenges of group network inference from intracranial EEG data). To deal with varying electrode implantation across subjects, we pooled connectivity estimates across all subjects after calculation

(apart from specific inter-subject analysis of SAB performance). We thus adopted a so-called *meta-patient* approach, a technique that has already been successfully applied elsewhere for the analysis of iEEG data (e.g., Gaillard et al., 2009). In addition, we performed a sensitivity analysis demonstrating that the obtained results are not driven by a single subject (Figure S2). Finally, the significance level was predetermined and set at $\alpha = 0.05$.

2.6 | Bootstrap testing

We used bootstrapping as a resampling technique for statistical testing of connectivity estimates. Bootstrapping employs random sampling with replacement from the distribution of interest and can be used to estimate the sampling distribution of almost any statistic (Efron & Tibshirani, 1994).

According to our predefined hypotheses, we first investigated the connectivity dynamics of brain networks. Specifically, we tested whether there is a significant increase in dynamic connectivity by comparing the mean connectivity at every time point to the baseline connectivity (from a time window centered at -75 ms) using a one-sided bootstrap hypothesis test for the difference in mean connectivity across all channel pairs with 10,000 bias-corrected bootstrap iterations. The bias-corrected implementation corrects for bias and skewness in the distribution of bootstrap estimates (see Penn, 2020, for a detailed description). The resulting p -values were corrected for multiple comparisons in the time domain with the Benjamini-Hochberg FDR algorithm (Benjamini & Hochberg, 1995).

Furthermore, we tested whether a network shows different connectivity in the top-down and bottom-up direction across the time course using a two-sided bootstrap hypothesis test for the difference in mean connectivity across all channel pairs with 10,000 stationary bootstrap iterations. Since the original bootstrap method is designed only for independent, identically distributed data and is not appropriate when data samples are dependent (such as time series), stationary bootstrap is a block technique that attempts to preserve the underlying autocorrelation (Lahiri, 2003). Stationary bootstrap wraps the data around in a circle (end-to-start) and a random window length that removes the edge effect of uneven weighing at the beginning and the end (Politis & White, 2004). Finally, we used the same test to examine the differences in mean connectivity between Hits and Correct rejections.

2.6.1 | Graph analyses

Two key concepts in graph theory are nodes and edges. In our analyses, nodes correspond to the 90 regions of the AAL atlas (Tzourio-Mazoyer et al., 2002). After assigning each channel to the AAL atlas region (Figure 2b), we discarded channels that did not belong to any region and regions with no recorded signal were discarded, which resulted in the coverage of 68 out of the 90 AAL atlas regions

(Table S1). Note that the perirhinal, parahippocampal, and entorhinal cortices are in the AAL atlas collectively referred to as the parahippocampal region.

The second constituent component of a graph is the set of edges. We defined an edge between two regions as the mean connectivity across all corresponding pairs of channels. Since every graph can be represented as an adjacency matrix, and since we used a sliding window technique, our dynamic brain networks thus corresponded to a set of adjacency matrices. Each adjacency matrix was based on data from all patients and represented an incomplete weighted directed graph.

Segregation and integration are two important network organization concepts relevant to human cognitive abilities. Segregation is the extent to which communication occurs primarily within tight-knit communities of regions. Conversely, integration is the ability of the network to integrate distributed information (Deco et al., 2015; Sporns, 2013). In this study, we assess integration by global efficiency and segregation by modularity (Cohen & D'Esposito, 2016). Since we based our networks on effective connectivity, we used directed counterparts of these measures. All analyses were performed using The Brain Connectivity Toolbox for MATLAB (Rubinov & Sporns, 2010).

2.7 | Modularity

Modularity quantifies the degree to which the network may be subdivided into densely interconnected communities that maximize the number of within-group edges and minimize the number of between-group edges (Newman, 2006). To estimate modularity, we applied the commonly used iterative Louvain algorithm to the adjacency matrix with the (default) resolution parameter of $\gamma = 1$ and random initial conditions for each time window of dynamic connectivity. A maximum of the modularity function across 10,000 randomly initialized algorithm runs was selected as the resulting modularity with its accompanying network partition (Sporns & Betzel, 2016). Since the community labeling can differ in each time window, we manually ensured consistent labeling across the time course. Furthermore, a node could be part of a different community in each time window. Therefore, we defined the final community allegiance as the most commonly assigned community across all time windows.

As we dynamically assign a community index to each node, we define the instability index as a relative number of node allegiance changes from the final community during the experiment.

2.8 | Efficiency

Global efficiency is defined as the average inverse shortest path between any two nodes (Latora & Marchiori, 2001). Considering that it is linearly dependent on connectivity strength between nodes, we normalized it by dividing it by the mean connectivity across all non-zero edges.

2.9 | Null model

The use and choice of a null model are crucial in graph analyses (Hindriks et al., 2016; Hlinka & Hadrava, 2015). To create a stationary system with an identical covariance structure, we used an amplitude-adjusted multivariate extension of Fourier surrogates (MVFS) that match the amplitude spectrum and amplitude distributions of recorded iEEG activities (Schreiber & Schmitz, 2000). Specifically, we repeated the above-described pipeline with 100 different realizations of MVFS of recorded iEEG data. This procedure generated a distribution of 100 modularity and efficiency values, serving as null distribution for our statistical testing.

In addition, we used MVFS to assess the significance of the difference in Hits and Correct rejections. To that end, we calculated Pearson's correlation between connectivity dynamics of Hits and Correct rejections for each detected community. The significance was based on the comparison with the null distribution generated by 1,000 correlations between MVFS of respective time series.

2.10 | Linking connectivity and subjects' performance

As the final step in our analyses, we set out to relate identified connectivity patterns with performance during the SAB task. To that end, we first calculated the mean connectivity in each identified community separately for each subject. We then quantified the association strength of the community-specific connectivity strength with d-prime and minimal reaction time. We quantified the magnitude of the linear relationship using Pearson's correlation. Associated *p*-values were FDR-corrected across all performed tests.

3 | RESULTS

Subjects underwent a fast visual recognition memory task. All 18 subjects performed well above chance (mean d-prime = 1.62 ± 0.44) (Table 1), and their performance did not differ from healthy controls (as reported in Despouy et al., 2020).

3.1 | Community analysis reveals three distinct communities underlying recognition memory

Our study aimed to investigate brain network dynamics supporting visual recognition memory. To detect networks driving successful recognition, we used the Louvain algorithm to detect community structures of the whole brain network. In other words, the Louvain algorithm partitioned the brain network into communities characteristic of strong connectivity between the regions within the community and weak connection with regions outside the community. Connectivity between two regions was defined as the average connectivity between all corresponding iEEG channels. We consistently identified

three communities at each time window (Figure 3a). Based on the most frequent allegiance of each node (cf. Methods), the first community comprised regions of the right temporal lobe as well as many frontal regions bilaterally. The second community was composed of regions in the left hemisphere, mainly in the temporal lobe and other parietal and frontal lobes. The third community comprised the left amygdala, parahippocampal, and inferior frontal gyri, as well as the right temporal sulcus. Consequently, since every channel belonged to a brain region, it was also assigned to a corresponding community.

As mentioned above, the first community primarily comprised regions in the right hemisphere. Concretely, 72% of all connections between iEEG channels corresponded to connections between right-hemisphere regions (Figure 3b). In contrast, the third community only included one region in the right hemisphere (64% of all iEEG channels corresponded to links between regions in the left hemisphere). The second community consisted of regions in both the left and right hemispheres, such as the left and right hippocampi (39% of channel connections were between hemispheres).

We then focused on the properties of each of the three communities, including their preference for top-down and bottom-up processes or stability. The communities differed significantly in the direction of information flow (i.e., the strength of connectivity in top-down and bottom-up directions) (Figure 3c). The first and second communities showed stronger connectivity in the bottom-up direction (two-sided bootstrap t -test $p_{\text{first}} = .04$, resp. $p_{\text{second}} = .05$). In comparison, the third community displayed significantly stronger connectivity in the top-down direction (two-sided bootstrap t -test $p = .0002$).

Finally, we probed the stability of the three communities. Even though the core of each community remained stable across the time course, some nodes changed network allegiance during the SAB test. Specifically, we found that the three communities differed in their stability (one-way ANOVA, $p < 10^{-3}$), with the first and third communities being very stable (Figure 3b). The second community was the least stable, meaning that its regions were relatively often members of the other two communities throughout the SAB test in comparison to the other two communities. In summary, we found two networks across the two hemispheres driven by bottom-up processes and a third network localized in the left hemisphere that supported top-down processes.

3.2 | Topology analyses reveal a link with community dynamics

After investigating the properties of the three communities, we focused on the connectivity dynamics of these sub-networks. Based on averaging connectivity across channels in each community, the first community showed the earliest connectivity increase compared with the baseline at around 115 ms (Figure 4a). The connectivity increase in the first community was followed by a significant connectivity increase in the third community at ~ 220 ms (Figure 4a). The connectivity of the second community remained comparable to the baseline. These results highlighted two networks with significant changes in connectivity dynamics underlying successful recognition.

As a last step of our connectivity analysis for the networks underlying successful recognition, we aimed to link significant changes in connectivity dynamics with the changes in brain network topology. We characterized the topology of the whole brain network using modularity (a measure of segregation) and efficiency (a measure of integration). In other words, we quantified how modularity and efficiency evolved over time. We observed a highly segregated network topology at 110 ms after stimulus onset. It then transitioned into a more integrated topology at ~ 220 ms (Figure 4b).

The global increase in modularity (MVFS $p < .05$, FDR-corrected) co-occurred with the significant connectivity increase in the first community at around 115 ms (Figure 4c). On the other side, the overall increase in efficiency was accompanied by the connectivity increase in the third community at 220 ms. Since the two communities differed in bottom-up and top-down connectivity, these results suggest that changes in overall brain network topology could be associated with network-specific changes in information flow.

3.3 | Network changes underlying successful recognition and correct rejection

According to our aims, we further investigated whether there was a difference in successful recognition of known versus unknown stimuli, that is, Hits and Correct rejections. We calculated Pearson's correlation between connectivity dynamics of Hits and Correct rejections for each community. We observed a strong positive correlation between connectivity dynamics in the first and third communities ($r_{\text{first}} = .52$, $r_{\text{second}} = -.21$, $r_{\text{third}} = .50$; Figure 5a). Only the correlation for the first community was significant ($p_{\text{first}} = .05$, $p_{\text{second}} = .75$, $p_{\text{third}} = .07$) based on the comparison with the null distribution generated by 1,000 correlations between MVFS of respective time series. In other words, for the first community, the connectivity dynamics during Hits resembled the connectivity dynamics of Correct rejection trials.

To complement the observed similarity in dynamics for the first community, we further compared connectivity strength between Hits and Correct rejections (Figure 5b). The first community displayed stronger connectivity for Hits compared with Correct rejections (bootstrap two-sided t -test p -value $< 10^{-5}$) across the timecourse of SAB test.

Finally, we assessed the relationship between the network dynamics and the subjects' performances. For each subject separately, we calculated the mean connectivity in each of the three identified communities. We then tested whether this subject-specific and network-specific connectivity strength was associated with test performance. To this end, we correlated d-prime and minimal reaction time with the connectivity strength. We found the connectivity strength in the third community to be associated with minimal reaction time ($r = -.51$, $p = .05$, FDR corrected). This result suggested that connectivity strength was linked with faster responses (Figure 5c). We did not observe a significant association with connectivity strength in other communities or with d-prime. In addition, we studied the relationship between the subject's sampling frequency and the mean connectivity in each of the three identified communities

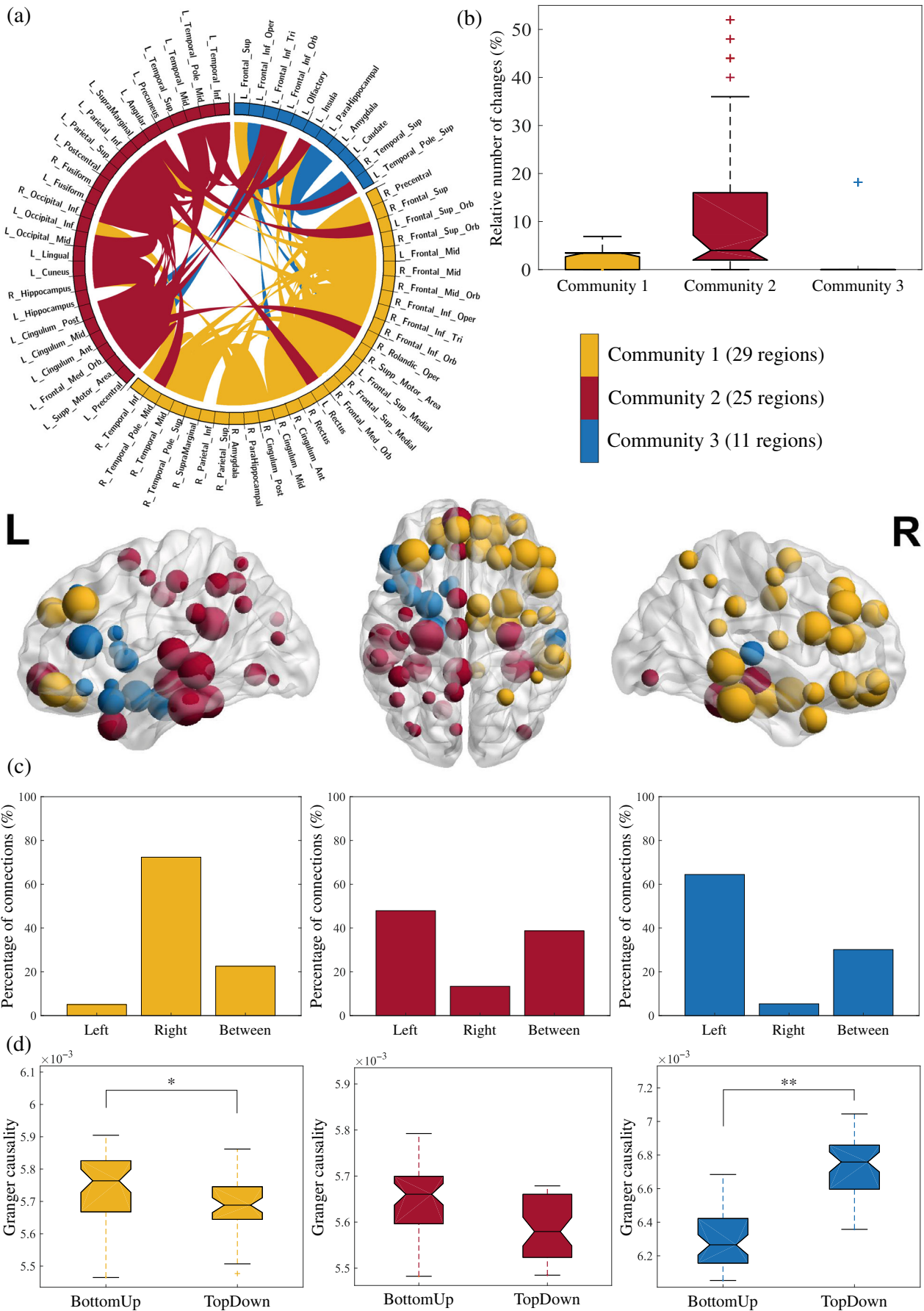


FIGURE 3 Legend on next page.

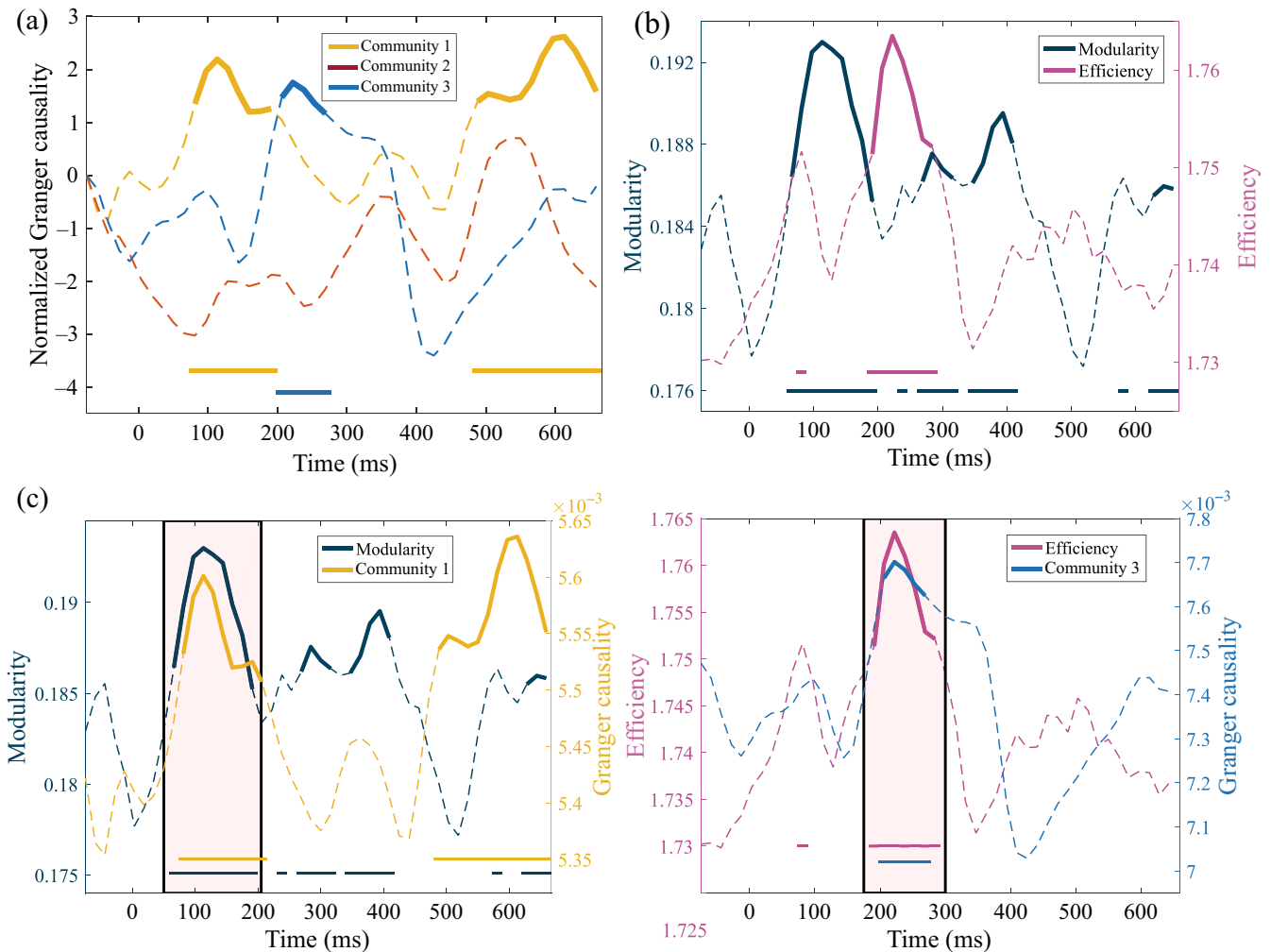


FIGURE 4 Changes in network topology are associated with changes in information flow. We quantified the connectivity dynamics in each community and the dynamics of brain topology. (a) Community connectivity dynamics. The plot depicts the mean connectivity in each of the three communities. The first community showed the earliest increase in connectivity (115 ms). The third community followed with a significant increase in connectivity at approximately 220 ms. The second community did not display any significant increase throughout the SAB test. (b) Dynamics of network modularity and efficiency. We dynamically quantified the overall brain network topology. At ~110 ms, the network showed a more modular topology. This segregated state is followed by a more integrated structure characterized by higher efficiency at 220 ms. Horizontal lines represent periods of significant increase/decrease based on MVFS testing with 100 iterations. (c) Two modes of information processing. The overall brain network properties (modularity, efficiency) were temporally related to the connectivity dynamics of two networks displaying significant connectivity changes. The first peak of modularity and significant connectivity increase in the first community appeared simultaneously at 110 ms. The first peak of efficiency at 220 ms occurred together with a significant connectivity increase in the third community. Solid lines indicate significant values. The rectangles highlight the time intervals of interest.

FIGURE 3 Community analyses of brain networks supporting recognition memory. (a) The Louvain algorithm consistently identified three main communities in our brain network. The first community comprised the right visual ventral stream, right subhippocampal structures, and frontal regions in both hemispheres. The second community comprised regions in the left MTL but also the right hippocampus. The third community comprised the left parahippocampal gyrus, left amygdala, and left inferior frontal gyrus. The size of the spheres in the brain graph corresponds to the nodal strength. The circular form (Krzywinski et al., 2009) shows only 3% of the strongest connections for visualization purposes. (b) Stability of the three communities. The three communities differed in their stability (one-way ANOVA, $p < 10^{-3}$). The second network showed the lowest stability, that is, the highest number of allegiance changes per node. (c) Community distribution across the hemispheres. The bar plots depict the relative number of iEEG connections in each hemisphere. The first community was anchored in the right hemisphere (72% of connections), while the third community was centered in the left hemisphere (64% of connections). The second community comprised regions from the left hemisphere, although some right-hemisphere regions were included as well. (d) Connectivity directionality in the communities assessed using Granger causality. The direction of information flow was significantly different between the three communities. The first community exhibited significantly stronger connectivity in the bottom-up direction. Conversely, the third community displayed significantly stronger connectivity in the top-down direction ($*p < .05$; $**p < .001$, FDR-corrected).

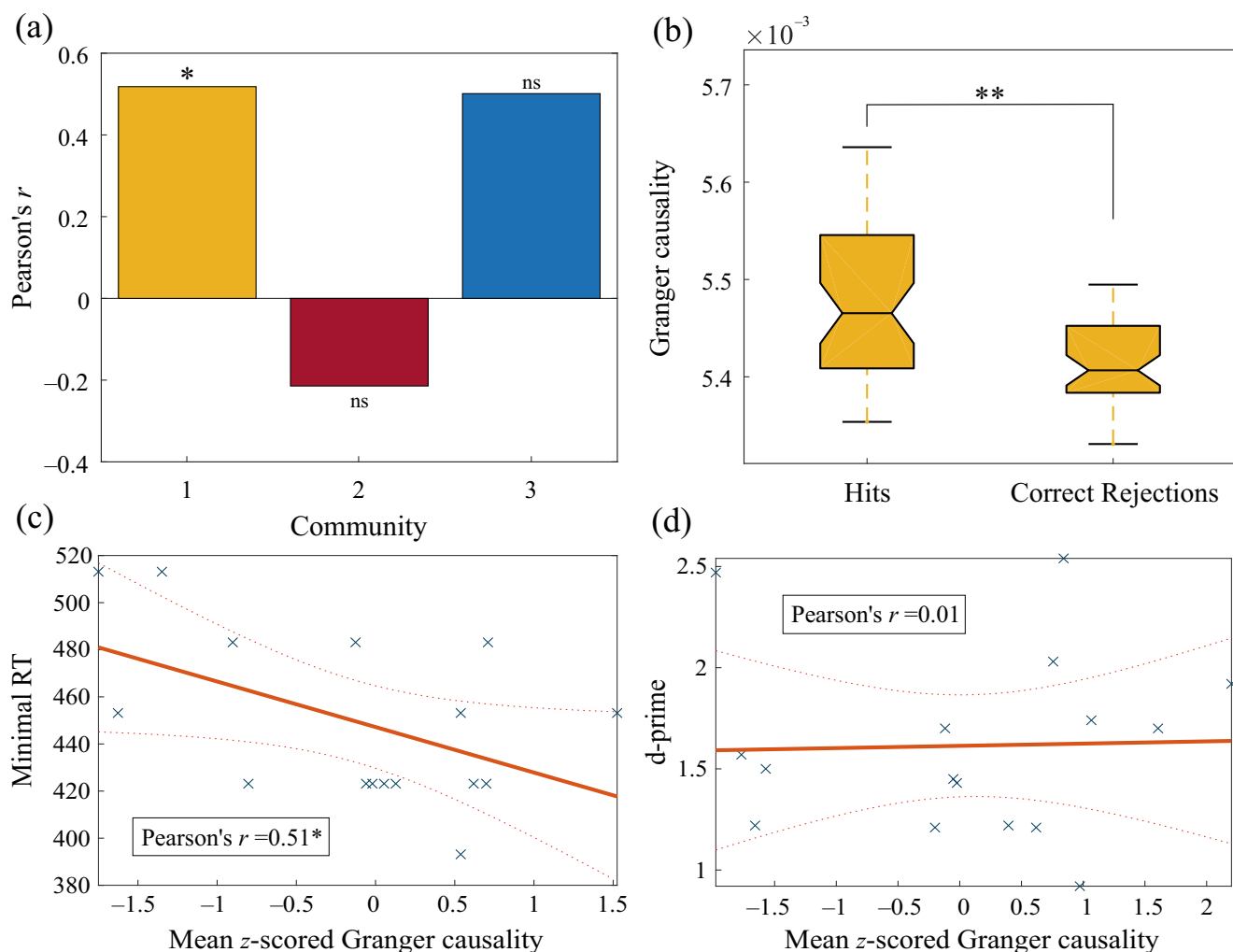


FIGURE 5 The relationship between community connectivity and performance. (a) Comparison of connectivity dynamics between Hits and Correct rejections. The temporal profiles of connectivity in the first community calculated for Hits were significantly correlated with connectivity dynamics in the same communities for Correct rejection trials ($r_{\text{first}} = .52$, $p_{\text{first}} = .05$; $r_{\text{second}} = -.21$, $p_{\text{second}} = .75$; $r_{\text{third}} = .50$, $p_{\text{third}} = .07$; $*p < .05$, ns = non-significant). (b) Comparison of connectivity strength between Hits and Correct rejections. The first community displayed significantly stronger connectivity for Hits compared with Correct rejections (** $p < .01$). (c) Relationship between community connectivity strength and reaction time. There was a strong negative correlation between the connectivity strength in the third community and minimal reaction time ($r = .51$, $p = .05$). (d) Relationship between community connectivity strength and performance. The relationship between the connectivity strength in the third community and d-prime was not significant ($r = .01$, $p > .05$). We also did not observe a significant relationship for the other two communities and minimal RT or d-prime.

(Figure 5c). Pearson's correlations did not reach significance for any of the three tests (all p -values $> .05$).

4 | DISCUSSION

This study investigated the dynamic reorganization of brain networks during a fast visual recognition memory task. We show that even within the first 300 ms after stimulus presentation, three large brain networks are intertwined, each with a specific topography, temporal dynamics, information flow, and stability. The first large-scale network involved the right visual ventral stream and frontal areas bilaterally. It was characterized by predominant bottom-up information flow,

peaking around 115 ms post-stimulus. Another involved network was centered around the left MTL but also included the right hippocampus. It did not display any significant change in connectivity dynamics. A third network involved predominantly left anterior regions and showed top-down information flow peaking at 220 ms. Furthermore, linking connectivity dynamics with network topology, the increase in bottom-up information flow was accompanied by a transition of the brain into a more segregated topology at 115 ms. Conversely, the increase in top-down information flow was associated with a transition to a more integrated topology around 220 ms. These analyses provide a picture of different functional networks that underlie fast visual recognition memory. More generally, it demonstrates that brain networks can shape very rapidly after stimulus onset and transition

quickly from one to the other, leading to different modes of information processing depending on different network configurations.

Our results revealed a highly modular state of the brain network and a community-localized significant connectivity increase during the early stages of the recognition memory task. These specific network properties appear in concordance with the modular organization of the ventral visual pathway (DiCarlo et al., 2012) and the necessity for efficient processing of visual stimuli (Maffei & Sessa, 2021). The architecture and dynamics of this first network are highly consistent with previous iEEG studies demonstrating early involvement of the right visual ventral pathway in visual recognition memory (Barbeau et al., 2017; Despouy et al., 2020). The extent of the first identified network was surprising as it comprised the visual ventral stream but also many frontal lobes areas bilaterally. However, it has already been established that frontal lobe regions are involved in object processing and recognition memory very early, as soon as 110 ms after stimulus presentation (Bar et al., 2006; Barbeau et al., 2008). In addition, there is strong support for the idea that the rapidity of the visual ventral stream is supported by feedforward mechanisms (DiCarlo et al., 2012), which appears to agree with our finding that the first community mainly involves bottom-up information flow. Overall, the first network could correspond to an early stage of relatively automatic processing of visual stimuli.

The early activation of frontal lobe regions has been proposed to prepare a stage for top-down processing (Bar et al., 2006). Staresina and Wimber (2019) have suggested that bottom-up, cue-driven input processes are followed by a reversal of the information flow to a top-down, memory-driven output process. Mashour et al. (2020) recently discussed the existence of a sudden divergence in brain activity at around 200 to 300 ms in various tasks. Similarly, independent recognition memory task studies have identified network changes occurring at around 240 ms (Barbeau et al., 2008; Goddard et al., 2016; Maillard et al., 2011). In addition, fMRI studies have consistently reported network reorganizations during cognitive tasks (Ekman et al., 2012; Shine et al., 2016). Overall, there is strong support for an early critical time point during which brain networks largely reorganize after initial stimulus processing. Here, our results highlight the simultaneous changes in global network topology and information flow that underlie or accompany these transitions. Specifically, we observed the transition from a highly segregated (115 ms) to a highly integrated state (220 ms) to be accompanied by the activation of a bottom-up network followed by the activation of a top-down network. The change in brain network topology stresses the brain's ability to quickly reconfigure dynamic networks in response to changing cognitive demands (Cohen & D'Esposito, 2016). Importantly, we observed reconfigurations occurring much faster than suggested in other memory studies, likely because our task was time-constrained (see Staresina & Wimber, 2019 for a review).

Westphal et al. (2017) suggested that efficient episodic (internally oriented) memory requires reduced modularity and a more integrated state, enabling higher information flow fluidity. Increased cognitive load has been shown to drive global integration, whereby the brain can adopt a more global workspace configuration (Ekman et al., 2012; Kitzbichler et al., 2011). The identified predominantly top-down network could thus be related to a host of explicit and controlled

cognitive processes, such as top-down modulation by valence or context effects (Ishai et al., 2006), the build-up of an internal representation of the stimulus (Rijsbergen & Schyns, 2009), access to a distributed semantic system and language (Burke et al., 2014), monitoring and controlling responses (Westphal et al., 2017), or more generally to conscious processing (Mashour et al., 2020). The variety and simultaneity of these adaptive processes could explain the need for integrated information processing. Petrovska et al. (2021) consistently stressed in an fMRI study of 1410 subjects the importance of left-lateralized networks in recognition memory (although the network encompassing the anterior ventral stream was, as expected, more right-lateralized), which is in agreement with the predominant left-lateralization of our identified network. In summary, given the different architecture of the top-down and bottom-up networks, as well as the different characteristics and cognitive processes they are thought to support, these networks may underlie highly different subjective experiences.

There have been many debates about the role of the hippocampus in recognition memory. Prior research suggests that the hippocampus may not be necessary when the response can be based on familiarity, as in our task design (Aggleton & Brown, 1999; Besson et al., 2012). Interestingly, both the right and left hippocampi belonged to the second network in this study, which did not show significant changes in connectivity dynamics. Although this result may need to be confirmed in future studies, it lends support to the idea that the hippocampus may not necessarily play a pivotal role in all declarative memory tasks (Basile et al., 2020).

Finally, linking behavioral responses with underlying network dynamics, we observed a strong negative correlation between minimal reaction times and the connectivity strength in the community characteristic of increased top-down connectivity. This observation implied that the strength of the connectivity is related to better brain processing efficiency. Behavioral responses require frontal lobes regions for confidence judgment, motor preparation, and decision (Bastin et al., 2019), which seems in line with the brain areas involved in this community (Despouy et al., 2020). As this was the only significant correlation between network properties and behavioral responses (e.g., no correlation was found with *d*-prime), it remains an interesting open question which of the two communities contributes most to the responses and whether they are underlined by different subjective experience (e.g., familiarity or recollection; Bastin et al., 2019; Besson et al., 2012). Future work should aim at clarifying these issues. It would also be highly informative to understand whether the identified network patterns are generic, that is, relatively replicable across different tasks, or specific to our task.

The limitations of this study followed the limitations inherent to all iEEG studies, that is, a relatively low number of subjects and subject-specific, tailored implantations that do not cover the entire brain. Obtaining generalizable findings across subjects necessitates subsequent channel selection based on criteria for which no golden standard exists. Furthermore, the definition of bottom-up and top-down processes corresponded to those operationally defined by Gailard et al. (2009). These definitions represented a simplification, and their relationship with feedforward and feedback processes remains

to be clarified. Future studies could benefit from frequency-resolved measures to detect networks that operate on specific frequencies (Maffei & Sessa, 2021). Adding frequency analyses was beyond this study's scope. Finally, it is worth reminding that epilepsy could impact the generalization of the results. However, as in all similar studies, we removed EEG periods contaminated with interictal epileptic activities. In addition, results based on iEEG are generally replicable across studies and centers (Hill et al., 2020).

In conclusion, this study revealed how different large-scale functional networks unfold early on and rapidly, that is, in <300 ms, during a cognitive task. It also highlighted specific characteristics of these networks and pointed to a critical transitional time point. It demonstrates that chronotomics studies based on intracerebral EEG could be particularly fruitful in clarifying functional networks' dynamics at the millisecond scale. Specific hypotheses could be tested explicitly in future work: for example, the notion that changes in network topology drive changes in information flow or the idea that network shaping could start even before stimulus presentation, given the rapidity of the changes we report. It will also be critical to examine the physiological mechanisms that enable modular coordination within networks or transitions between different networks.

AUTHOR CONTRIBUTIONS

Emmanuel J. Barbeau conceived and designed the experiments. Jakub Kopal, Jaroslav Hlinka designed the data analyses. Elodie Despouy performed the experiments. Jakub Kopal analyzed the data. Jonathan Curot, Luc Valton, Jean-Christophe Sol, and Marie Denuelle contributed reagents/materials/analysis tools. Jakub Kopal, Jaroslav Hlinka, and Emmanuel J. Barbeau wrote the paper with input from all authors.

ACKNOWLEDGEMENTS

This work has been supported by Campus France grant No. 44815QG, the Czech Science Foundation project No. 19-11753S, Ministry of Health Czech Republic – DRO 2021 (“National Institute of Mental Health – NIMH, IN: 00023752”) and from the Specific university research – grant No. A2 FCHI 2018 012.

CONFLICT OF INTEREST STATEMENT

The authors declare no competing financial interest.

DATA AVAILABILITY STATEMENT

The data that support the findings of this study are available on request from the corresponding author. The data are not publicly available due to privacy or ethical restrictions.

ORCID

Jaroslav Hlinka  <https://orcid.org/0000-0003-1402-1470>

REFERENCES

- Aggleton, J. P., & Brown, M. W. (1999). Episodic memory, amnesia, and the hippocampal-anterior thalamic axis. *Behavioral and Brain Sciences*, 22(3), 425–444. <https://doi.org/10.1017/s0140525x99002034>
- Bar, M., Kassam, K. S., Ghuman, A. S., Boshyan, J., Schmid, A. M., Dale, A. M., Hämäläinen, M. S., Marinkovic, K., Schacter, D. L., Rosen, B. R., & Halgren, E. (2006). Top-down facilitation of visual recognition. *Proceedings of the National Academy of Sciences*, 103, 449–454. <https://doi.org/10.1073/pnas.0507062103>
- Barbeau, E. J., Chauvel, P., Moulin, C. J. A., Regis, J., & Liégeois-Chauvel, C. (2017). Hippocampus duality: Memory and novelty detection are subserved by distinct mechanisms. *Hippocampus*, 27, 405–416. <https://doi.org/10.1002/hipo.22699>
- Barbeau, E. J., Taylor, M. J., Regis, J., Marquis, P., Chauvel, P., & Liégeois-Chauvel, C. (2008). Spatio temporal dynamics of face recognition. *Cerebral Cortex*, 18, 997–1009. <https://doi.org/10.1093/cercor/bhm140>
- Barnett, L., & Seth, A. K. (2014). The MVGC multivariate granger causality toolbox: A new approach to granger causal inference. *Journal of Neuroscience Methods*, 223, 50–68. <https://doi.org/10.1016/j.jneumeth.2013.10.018>
- Barragan-Jason, G., Cauchoix, M., & Barbeau, E. (2015). The neural speed of familiar face recognition. *Neuropsychologia*, 75, 390–401. <https://doi.org/10.1016/j.neuropsychologia.2015.06.017>
- Basile, B. M., Templer, V. L., Gazes, R. P., & Hampton, R. R. (2020). Preserved visual memory and relational cognition performance in monkeys with selective hippocampal lesions. *Science Advances*, 6(29), eaaz0484. <https://doi.org/10.1126/sciadv.aaz0484>
- Bassett, D. S., Wymbs, N. F., Porter, M. A., Mucha, P. J., Carlson, J. M., & Grafton, S. T. (2011). Dynamic reconfiguration of human brain networks during learning. *Proceedings of the National Academy of Sciences*, 108, 7641–7646. <https://doi.org/10.1073/pnas.1018985108>
- Bastin, C., Besson, G., Simon, J., Delhaye, E., Geurten, M., Willems, S., & Salmon, E. (2019). An integrative memory model of recollection and familiarity to understand memory deficits. *Behavioral and Brain Sciences*, 42, e281. <https://doi.org/10.1017/S0140525X19000621>
- Benjamini, Y., & Hochberg, Y. (1995). Controlling the false discovery rate: A practical and powerful approach to multiple testing. *Journal of the Royal Statistical Society, Series B*, 57(1), 289–300. <https://doi.org/10.1111/j.2517-6161.1995.tb02031>
- Besson, G., Ceccaldi, M., Didic, M., & Barbeau, E. J. (2012). The speed of visual recognition memory. *Visual Cognition*, 20, 1131–1152. <https://doi.org/10.1080/13506285.2012.724034>
- Brady, T. F., Konkle, T., Alvarez, G. A., & Oliva, A. (2008). Visual long-term memory has a massive storage capacity for object details. *Proceedings of the National Academy of Sciences*, 105, 14325–14329. <https://doi.org/10.1073/pnas.0803390105>
- Braun, U., Schäfer, A., Walter, H., Erk, S., Romanczuk-Seiferth, N., Haddad, L., Schweiger, J. I., Grimm, O., Heinz, A., Tost, H., Meyer-Lindenberg, A., & Bassett, D. S. (2015). Dynamic reconfiguration of frontal brain networks during executive cognition in humans. *Proceedings of the National Academy of Sciences*, 112, 11678–11683. <https://doi.org/10.1073/pnas.1422487112>
- Brown, M. W., & Aggleton, J. P. (2001). Recognition memory: What are the roles of the perirhinal cortex and hippocampus? *Nature Reviews Neuroscience*, 2, 51–61. <https://doi.org/10.1038/35049064>
- Burke, J. F., Long, N. M., Zaghoul, K. A., Sharan, A. D., Sperling, M. R., & Kahana, M. J. (2014). Human intracranial high-frequency activity maps episodic memory formation in space and time. *NeuroImage*, 85, 834–843. <https://doi.org/10.1016/j.neuroimage.2013.06.067>
- Calhoun, V. D., Miller, R., Pearlson, G., & Adali, T. (2014). The chronnectome: Time-varying connectivity networks as the next frontier in fMRI data discovery. *Neuron*, 84(2), 262–274. <https://doi.org/10.1016/j.neuron.2014.10.015>
- Cohen, J. R., & D'Esposito, M. (2016). The segregation and integration of distinct brain networks and their relationship to cognition. *The Journal of Neuroscience*, 36, 12083–12094. <https://doi.org/10.1523/jneurosci.2965-15.2016>

- Deco, G., Tononi, G., Boly, M., & Kringelbach, M. L. (2015). Rethinking segregation and integration: Contributions of whole-brain modelling. *Nature Reviews Neuroscience*, 16, 430–439. <https://doi.org/10.1038/nrn3963>
- Despoux, E., Curot, J., Deudon, M., Gardy, L., Denuelle, M., Sol, J.-C., Lotterie, J.-A., Valton, L., & Barbeau, E. J. (2020). A fast visual recognition memory system in humans identified using intracerebral ERP. *Cerebral Cortex*, 30, 2961–2971. <https://doi.org/10.1093/cercor/bhz287>
- DiCarlo, J., Zoccolan, D., & Rust, N. (2012). How does the brain solve visual object recognition? *Neuron*, 73, 415–434. <https://doi.org/10.1016/j.neuron.2012.01.010>
- Efron, B., & Tibshirani, R. J. (1994). *An introduction to the bootstrap*. CRC Press.
- Eichenbaum, H., Yonelinas, A. P., & Ranganath, C. (2007). The medial temporal lobe and recognition memory. *Annual Review of Neuroscience*, 30, 123–152. <https://doi.org/10.1146/annurev.neuro.30.051606.094328>
- Eickhoff, S. B., Stephan, K. E., Mohlberg, H., Grefkes, C., Fink, G. R., Amunts, K., & Zilles, K. (2005). A new SPM toolbox for combining probabilistic cytoarchitectonic maps and functional imaging data. *NeuroImage*, 25, 1325–1335. <https://doi.org/10.1016/j.neuroimage.2004.12.034>
- Ekman, M., Derrfuss, J., Tittgemeyer, M., & Fiebach, C. J. (2012). Predicting errors from reconfiguration patterns in human brain networks. *Proceedings of the National Academy of Sciences*, 109, 16714–16719. <https://doi.org/10.1073/pnas.1207523109>
- Elger, C. E., Grunwald, T., Lehnertz, K., Kutas, M., Helmstaedter, C., Brockhaus, A., van Roost, D., & Heinze, H. J. (1997). Human temporal lobe potentials in verbal learning and memory processes. *Neuropsychologia*, 35, 657–667. [https://doi.org/10.1016/s0028-3932\(96\)00110-8](https://doi.org/10.1016/s0028-3932(96)00110-8)
- Gaillard, R., Dehaene, S., Adam, C., Clémenceau, S., Hasboun, D., Baulac, M., Cohen, L., & Naccache, L. (2009). Converging intracranial markers of conscious access. *PLoS Biology*, 7(3), e1000061. <https://doi.org/10.1371/journal.pbio.1000061>
- Goddard, E., Carlson, T. A., Dermody, N., & Woolgar, A. (2016). Representational dynamics of object recognition: Feedforward and feedback information flows. *NeuroImage*, 128, 385–397. <https://doi.org/10.1016/j.neuroimage.2016.01.006>
- Gonzalez, A., Hutchinson, J. B., Uncapher, M. R., Chen, J., LaRocque, K. F., Foster, B. L., Rangarajan, V., Parvizi, J., & Wagner, A. D. (2015). Electrocortical activity reveals the temporal dynamics of posterior parietal cortical activity during recognition memory decisions. *Proceedings of the National Academy of Sciences*, 112, 11066–11071. <https://doi.org/10.1073/pnas.1510749112>
- Guerin, S. A., & Miller, M. B. (2009). Lateralization of the parietal old/new effect: An event-related fMRI study comparing recognition memory for words and faces. *NeuroImage*, 44(1), 232–242. <https://doi.org/10.1016/j.neuroimage.2008.08.035>
- Hill, P. F., King, D. R., Lega, B. C., & Rugg, M. D. (2020). Comparison of fMRI correlates of successful episodic memory encoding in temporal lobe epilepsy patients and healthy controls. *NeuroImage*, 207, 116397. <https://doi.org/10.1016/j.neuroimage.2019.116397>
- Hindriks, R., Adhikari, M. H., Murayama, Y., Ganzetti, M., Mantini, D., Logothetis, N. K., & Deco, G. (2016). Can sliding-window correlations reveal dynamic functional connectivity in resting-state fMRI? *NeuroImage*, 127, 242–256. <https://doi.org/10.1016/j.neuroimage.2015.11.055>
- Hlinka, J., & Hadrava, M. (2015). On the danger of detecting network states in white noise. *Frontiers in Computational Neuroscience*, 9, 11. <https://doi.org/10.3389/fncom.2015.00011>
- Hoppstädter, M., Baeuchl, C., Diener, C., Flor, H., & Meyer, P. (2015). Simultaneous EEG–fMRI reveals brain networks underlying recognition memory ERP old/new effects. *NeuroImage*, 116, 112–122. <https://doi.org/10.1016/j.neuroimage.2015.05.026>
- Hutchison, R. M., Womelsdorf, T., Allen, E. A., Bandettini, P. A., Calhoun, V. D., Corbetta, M., Della Penna, S., Duyn, J. H., Glover, G. H., Gonzalez-Castillo, J., Handwerker, D. A., Keilholz, S., Kiviniemi, V., Leopold, D. A., de Pasquale, F., Sporns, O., Walter, M., & Chang, C. (2013). Dynamic functional connectivity: Promise, issues, and interpretations. *NeuroImage*, 80, 360–378. <https://doi.org/10.1016/j.neuroimage.2013.05.079>
- Ishai, A., Bickle, P. C., & Ungerleider, L. G. (2006). Temporal dynamics of face repetition suppression. *Brain Research Bulletin*, 70, 289–295. <https://doi.org/10.1016/j.brainresbull.2006.06.002>
- Kitzbichler, M. G., Henson, R. N. A., Smith, M. L., Nathan, P. J., & Bullmore, E. T. (2011). Cognitive effort drives workspace configuration of human brain functional networks. *Journal of Neuroscience*, 31, 8259–8270. <https://doi.org/10.1523/jneurosci.0440-11.2011>
- Krzywinski, M., Schein, J., Birol, I., Connors, J., Gascoyne, R., Horsman, D., Jones, S. J., & Marra, M. A. (2009). Circos: An information aesthetic for comparative genomics. *Genome Research*, 19, 1639–1645. <https://doi.org/10.1101/gr.092759.109>
- Lachaux, J. P., Rudrauf, D., & Kahane, P. (2003). Intracranial EEG and human brain mapping. *Journal of Physiology, Paris*, 97, 613–628. <https://doi.org/10.1016/j.jphysparis.2004.01.018>
- Lahiri, S. N. (2003). *Resampling methods for dependent data*. Springer series in statistics. Springer-Verlag. <https://doi.org/10.1007/978-1-4757-3803-2>
- Larzabal, C., Tramon, E., Muratot, S., Thorpe, S. J., & Barbeau, E. J. (2018). Extremely long-term memory and familiarity after 12 years. *Cognition*, 170, 254–262. <https://doi.org/10.1016/j.cognition.2017.10.009>
- Latora, V., & Marchiori, M. (2001). Efficient behavior of small-world networks. *Physical Review Letters*, 87, 198701. <https://doi.org/10.1103/PhysRevLett.87.198701>
- Maffei, A., & Sessa, P. (2021). Time-resolved connectivity reveals the “how” and “when” of brain networks reconfiguration during face processing. *NeuroImage: Reports*, 1(2), 100022. <https://doi.org/10.1016/j.ynirp.2021.100022>
- Maillard, L., Barbeau, E. J., Baumann, C., Koessler, L., Bénar, C., Chauvel, P., & Liégeois-Chauvel, C. (2011). From perception to recognition memory: Time course and lateralization of neural substrates of word and abstract picture processing. *Journal of Cognitive Neuroscience*, 23, 782–800. <https://doi.org/10.1162/jocn.2010.21434>
- Mashour, G. A., Roelfsema, P., Changeux, J.-P., & Dehaene, S. (2020). Conscious processing and the global neuronal workspace hypothesis. *Neuron*, 105(5), 776–798. <https://doi.org/10.1016/j.neuron.2020.01.026>
- Meunier, D., Fonlupt, P., Saive, A.-L., Plailly, J., Ravel, N., & Royet, J.-P. (2014). Modular structure of functional networks in olfactory memory. *NeuroImage*, 95, 264–275. <https://doi.org/10.1016/j.neuroimage.2014.03.041>
- Milner, B. (1972). Disorders of learning and memory after temporal lobe lesions in man. *Neurosurgery*, 19, 421–446. <https://doi.org/10.1093/neurosurgery/19.CNsuppl1.421>
- Newman, M. E. J. (2006). Modularity and community structure in networks. *Proceedings of the National Academy of Sciences of the United States of America*, 103, 8577–8582. <https://doi.org/10.1073/pnas.0601602103>
- Patterson, K., & Bradshaw, J. L. (1975). Differential hemispheric mediation of nonverbal visual stimuli. *Journal of Experimental Psychology: Human Perception and Performance*, 1, 246–252. <https://doi.org/10.1037/0096-1523.1.3.246>
- Penn, A. (2020). iboot: Iterated bootstrap for small samples and samples with complex dependence structures. <https://github.com/acp29/iboot> <https://doi.org/10.5281/ZENODO.3992393>
- Petrovska, J., Loos, E., Coynel, D., Egli, T., Papassotiropoulos, A., de Quervain, D. J., & Milnik, A. (2021). Recognition memory performance can be estimated based on brain activation networks. *Behavioural Brain Research*, 408, 113285. <https://doi.org/10.1016/j.bbr.2021.113285>

- Pidnebesna, A., Sanda, P., Kalina, A., Hammer, J., Marusic, P., Vlcek, K., & Hlinka, J. (2022). Tackling the challenges of group network inference from intracranial EEG data. *Frontiers in Neuroscience*, *16*, 1061867. <https://doi.org/10.3389/fnins.2022.1061867>
- Politis, D. N., & White, H. (2004). Automatic block-length selection for the dependent bootstrap. *Econometric Reviews*, *23*, 53–70. <https://doi.org/10.1081/ETC-120028836>
- Preti, M. G., Bolton, T. A., & Van De Ville, D. (2017). The dynamic functional connectome: State-of-the-art and perspectives. *NeuroImage*, *160*, 41–54. <https://doi.org/10.1016/j.neuroimage.2016.12.061>
- Rijsbergen, N. J. V., & Schyns, P. G. (2009). Dynamics of trimming the content of face representations for categorization in the brain. *PLoS Computational Biology*, *5*, e1000561. <https://doi.org/10.1371/journal.pcbi.1000561>
- Rousselle, G. A., Thorpe, S. J., & Fabre-Thorpe, M. (2004). Processing of one, two or four natural scenes in humans: The limits of parallelism. *Vision Research*, *44*(9), 877–894. <https://doi.org/10.1016/j.visres.2003.11.014>
- Rubinov, M., & Sporns, O. (2010). Complex network measures of brain connectivity: Uses and interpretations. *NeuroImage*, *52*, 1059–1069. <https://doi.org/10.1016/j.neuroimage.2009.10.003>
- Schreiber, T., & Schmitz, A. (2000). Surrogate time series. *Physica D: Non-linear Phenomena*, *142*, 346–382. [https://doi.org/10.1016/S0167-2789\(00\)00043-9](https://doi.org/10.1016/S0167-2789(00)00043-9)
- Seth, A. K., Barrett, A. B., & Barnett, L. (2015). Granger causality analysis in neuroscience and neuroimaging. *Journal of Neuroscience*, *35*, 3293–3297. <https://doi.org/10.1523/jneurosci.4399-14.2015>
- Shine, J. M., Bissett, P. G., Bell, P. T., Koyejo, O., Balsters, J. H., Gorgolewski, K. J., Moodie, C. A., & Poldrack, R. A. (2016). The dynamics of functional brain networks: Integrated network states during cognitive task performance. *Neuron*, *92*, 544–554. <https://doi.org/10.1016/j.neuron.2016.09.018>
- Sporns, O. (2007). Brain connectivity. *Scholarpedia*, *2*, 4695. <https://doi.org/10.4249/scholarpedia.4695>
- Sporns, O. (2011). The non-random brain: Efficiency, economy, and complex dynamics. *Frontiers in Computational Neuroscience*, *5*, 5. <https://doi.org/10.3389/fncom.2011.00005>
- Sporns, O. (2013). Network attributes for segregation and integration in the human brain. *Current Opinion in Neurobiology*, *23*, 162–171. <https://doi.org/10.1016/j.conb.2012.11.015>
- Sporns, O., & Betzel, R. F. (2016). Modular brain networks. *Annual Review of Psychology*, *67*, 613–640. <https://doi.org/10.1146/annurev-psych-122414-033634>
- Staresina, B. P., Fell, J., Do Lam, A. T. A., Axmacher, N., & Henson, R. N. (2012). Memory signals are temporally dissociated in and across human hippocampus and perirhinal cortex. *Nature Neuroscience*, *15*, 1167–1173. <https://doi.org/10.1038/nn.3154>
- Staresina, B. P., & Wimber, M. (2019). A neural chronometry of memory recall. *Trends in Cognitive Sciences*, *23*(12), 1071–1085. <https://doi.org/10.1016/j.tics.2019.09.011>
- Tzourio-Mazoyer, N., Landeau, B., Papathanassiou, D., Crivello, F., Etard, O., Delcroix, N., Mazoyer, B., & Joliot, M. (2002). Automated anatomical labeling of activations in SPM using a macroscopic anatomical parcellation of the MNI MRI single-subject brain. *NeuroImage*, *15*, 273–289. <https://doi.org/10.1006/nimg.2001.0978>
- VanRullen, R., & Thorpe, S. J. (2001). Is it a bird? Is it a plane? Ultra-rapid visual categorisation of natural and artificial objects. *Perception*, *30*(6), 655–668. <https://doi.org/10.1068/p3029>
- Varela, F., Lachaux, J.-P., Rodriguez, E., & Martinerie, J. (2001). The brainweb: Phase synchronization and largescale integration. *Nature Reviews Neuroscience*, *2*, 229–239. <https://doi.org/10.1038/35067550>
- Westphal, A. J., Wang, S., & Rissman, J. (2017). Episodic memory retrieval benefits from a less modular brain network organization. *Journal of Neuroscience*, *37*, 3523–3531. <https://doi.org/10.1523/jneurosci.2509-16.2017>

SUPPORTING INFORMATION

Additional supporting information can be found online in the Supporting Information section at the end of this article.

How to cite this article: Kopal, J., Hlinka, J., Despouy, E., Valton, L., Denuelle, M., Sol, J.-C., Curot, J., & Barbeau, E. J. (2023). Large-scale network dynamics underlying the first few hundred milliseconds after stimulus presentation: An investigation of visual recognition memory using iEEG. *Human Brain Mapping*, *44*(17), 5795–5809. <https://doi.org/10.1002/hbm.26477>